

This document is the post-print version of the paper
“CFD simulation of the magnetohydrodynamic flow inside
the WCLL breeding blanket module” published on Fusion
Engineering and Design. Doi: 10.1016/j.fusengdes.2017.05.098

CFD simulation of the magnetohydrodynamic flow inside the WCLL breeding blanket module

Alessandro Tassone^{a*}, Gianfranco Caruso^a, Alessandro Del Nevo^b, Ivan Di Piazza^b

^a DIAEE Nuclear Section - Sapienza University of Rome, Corso Vittorio Emanuele II, 244, 00186, Roma, Italy

^b ENEA CR Brasimone, 40032, Camugnano (BO), Italy

Abstract

The interaction between the molten metal and the plasma-containing magnetic field in the breeding blanket causes the onset of a magnetohydrodynamic (MHD) flow. To properly design the blanket, it is important to quantify how and how much the flow features are modified compared with an ordinary hydrodynamic flow. This paper aims to characterize the evolution of the fluid inside one of the proposed concepts for DEMO, the Water-Cooled Lithium Lead (WCLL), focusing on the central cell of the equatorial outboard module. A preliminary validation was required to gauge the capability of ANSYS CFX to deal with MHD problems. The buoyant and pressure-driven fully developed laminar flows in a square duct were selected as benchmarks. Numerical results were compared with theoretical solutions and an excellent agreement was found. The channel analysis was realized on a simplified version of the latest available design geometry, developed by ENEA, for $M \leq 1000$. The simulation highlighted the formation of high velocity jets close to the baffle and the onset of an asymmetrical potential distribution.

Keywords: MHD, magnetohydrodynamic flow, CFD, breeding blanket, DEMO fusion reactor

1. Introduction

The Breeding Blanket Project (WPBB) started in the 2014 to develop conceptual designs for the prototype DEMO reactor. The Water-Cooled Lithium Lead (WCLL) is one of the four blankets actually under investigation and the only one to employ water as coolant for both the breeder zone and the first wall. An updated design with modular geometry and a revised layout of the coolant hydraulic circuit was released in the 2015 by ENEA [1].

The issues to be addressed by the project are numerous. One of the most compelling is the interaction between the lithium-lead (LiPb) and the magnetic field employed for the plasma confinement. This phenomenon modifies the features of the fluid flow, therefore called magnetohydrodynamic. Lorentz forces arise in the bulk of the fluid, obstructing its movement, and cause huge increments in the pressure drops. Moreover, the velocity distribution undergoes drastically alterations with the appearance of jets, slug flow in the core, suppression of turbulent structures, etc. These effects must be analyzed to ensure the meeting of the DEMO specifications by the WCLL [2].

This study aims to investigate the features of the MHD flow in the elementary cell of the WCLL and to provide a first estimate of the pressure drops. Despite the efforts

of the fusion community, a dedicated computational MHD code able to simulate the relevant phenomena in the parameter range of the blanket is still unavailable [3]. For the purpose of this work, the ANSYS CFX was employed. A preliminary validation with benchmark cases was conducted to gauge the capabilities of the code.

2. Formulation

The Navier-Stokes equations must be modified to represent the interaction between the conductive fluid and the applied magnetic field. In the following, the electric potential formulation of the MHD governing equations would be employed. If the fluid is a liquid metal, its Reynolds magnetic number (R_m) $\ll 1$ and the influence of the induced magnetic field can be neglected [4]. For a steady, isothermal and incompressible flow the continuity and momentum equations can be written as

$$\nabla \cdot \vec{v} = 0 \quad (1)$$

$$(\vec{v} \cdot \nabla) \vec{v} = -\frac{1}{\rho} \nabla p + \nu \nabla^2 \vec{v} + \frac{1}{\rho} \vec{j} \times \vec{B} + \vec{S}_m \quad (2)$$

where the third term on the right side of (2) represents the Lorentz force and the fourth a momentum source, e.g. due to buoyancy forces. The electric current density \vec{j} is

*Corresponding author:

Email address: alessandro.tassone@uniroma1.it (Alessandro Tassone^a)

obtained by the Ohm's law and the charge conservation equations

$$\vec{j} = -\nabla\phi + \vec{v} \times \vec{B} \quad (3)$$

$$\nabla \cdot \vec{j} = 0 \quad (4)$$

Combining (3) and (4), it is found the Poisson equation

$$\nabla^2\phi = \nabla \cdot (\vec{v} \times \vec{B}) \quad (5)$$

which, once solved, provides the electric potential ϕ distribution and, through (3), the current density one.

Two fundamental parameters influence the flow features: the Hartmann number (M) and the wall conductance ratio (c). The Hartmann number is proportional to the ratio between the electromagnetic and the viscous forces and can be expressed as

$$M = BL\sqrt{\frac{\sigma}{\mu}} \quad (6)$$

where B is the intensity of the applied magnetic field; σ and μ are the electrical conductivity and dynamic viscosity of the fluid; L is the flow length scale (half-width of the duct in the toroidal direction). For a square duct, two different classes of boundary layers form alongside the walls parallel (side walls) and the ones perpendicular (Hartmann walls) to the magnetic field direction. The scale of these is expressed by the relations $\delta_S = 1/\sqrt{M}$ and $\delta_H = 1/M$.

The wall conductance ratio represents the influence of the duct wall conductivity on the flow features

$$c = \frac{\sigma_w}{\sigma} \frac{t}{L} \quad (7)$$

where σ_w is the electrical conductivity and t the thickness of the wall. Insulating walls lead to a higher resistance for the current paths and, therefore, to lower Lorentz forces compared with duct with conductive walls.

3. Code validation

Two 2D steady-state flow benchmarks were employed: a buoyant flow for a pair of differentially heated walls and an adiabatic pressure-driven flow. Analytical solutions [5][6][7] and numerical data [8][9] were used to validate the results. The quality of these was measured with two indexes: a local error (evaluated on the peak velocity value) and an integral error. For the latter, it was considered the non-dimensional flow rate \dot{Q} for the forced convection case [3], whereas for the buoyant flow benchmark it refers to the integral of the side wall velocity profile. Simulations were conducted with M ranging from 10^2 to 10^4 for both insulating and conductive walls. Selected results are presented in Figure 1 and 2 with an overview available in Table 1. More details about the validation methodology are provided in [10].

Table 1

Validation results for peak (p.e.) and integral error (i.e.)

Buoyant test case				P-driven test case			
c	M	p.e.[%]	i.e.[%]	c	M	p.e.[%]	i.e.[%]
0	100	0.68		0	500		0.54
	400	4.08	n.a.		5000	n.a.	0.21
	1000	2.08			10000		0.01
					15000		0.44
∞	100	2.01	0.79	∞	100	2.85	0.03
	400	1.26	1.49		400	3.08	0.14
	1000	2.20	1.46		1000	7.14	0.13

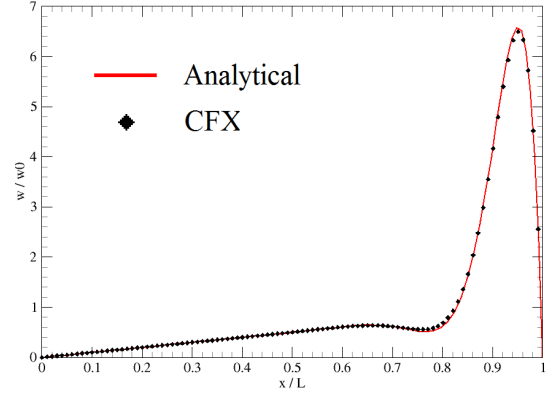


Fig. 1. Buoyant case side wall velocity profile for $M = 4 \cdot 10^2$ and $c = \infty$. The profile was scaled according to [8]

4. WCLL cell analysis

The geometry of the blanket elementary cell described in the WCLL Design 2015 was employed to perform the study [1]. To focus the investigation on the breeding zone, manifold and coolant pipes were removed. The LiPb fluid was assumed as isothermal at $T = 599$ K with properties calculated according to the correlations reported by Jauch et al. [11]. The channel walls were modeled by Eurofer97 at the same temperature, according to the correlations in Mergia & Boukos [12].

The magnetic field was considered constant with an

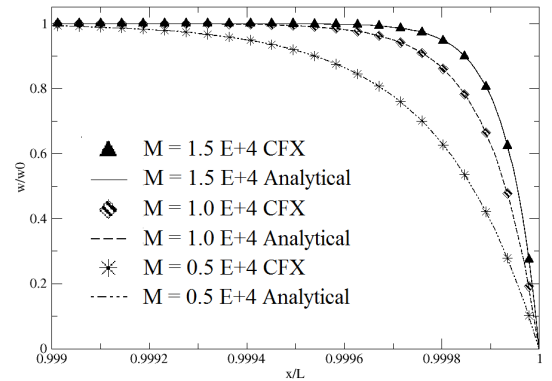


Fig. 2. Pressure driven case Hartmann wall velocity profile from $M = 0.5 \cdot 10^4$ to $1.5 \cdot 10^4$ and $c = 0$. The profile was scaled with the center duct velocity.

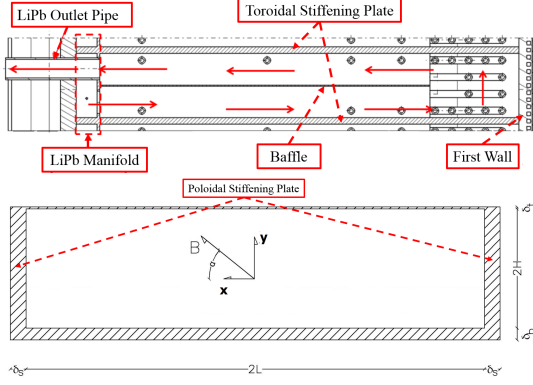


Fig. 3. WCLL elementary cell with LiPb flow path highlighted, radial-poloidal cross-section, (top) and inlet duct, poloidal-toroidal cross-section (bottom)

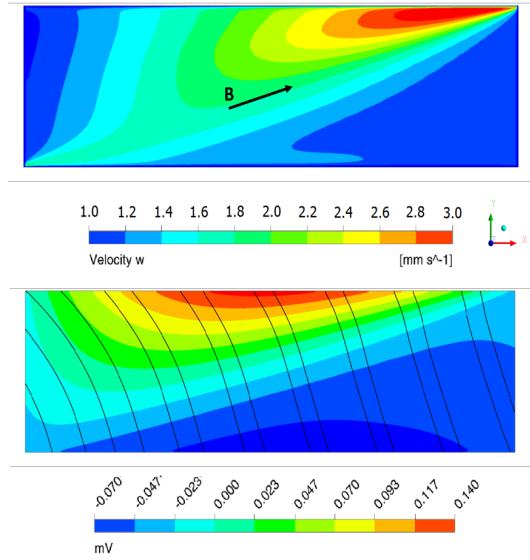


Fig. 4. Velocity (top) and potential contour with current streamlines (bottom) for the inlet duct, toroidal-poloidal cross-section, at $M = 980$

inclination $\alpha = 16^\circ$ on the toroidal axis. The intensity was scaled down from the blanket operative value¹ to the range $M = 490 - 980$. To improve the convergence speed and numerical stability of the model, two dummy walls were rendered in the bend region to avoid the breeder movements toward the nearby (not-modeled) channels. These were considered as formed by solid LiPb, electrically equivalent to the fluid.

The flow path described by the liquid metal is shown in Figure 3. At the inlet the flow is assumed to be fully developed with an average velocity $u_0 = 1.55$ mm/s and $Re = 787$. A zero pressure boundary condition was employed for the outlet. The duct walls are conductive, therefore eq. (5) is solved in both the fluid and solid domain, which are coupled assuming the conservation at the interface of current density and electric potential. Parameters

Table 2

WCLL simulation parameters. The Hartmann number range investigated in the study is reported in brackets

Duct [mm]			Wall		Flow	
			δ [mm]	c	M	Re
$L(\text{tor})$	117	Baffle	1	0.0125	9800	787
$H(\text{pol})$	33	SP(pol)	8	0.1000	(490-980)	
$Z(\text{rad})$	800	SP(tor)	6	0.0750		

of the model are available in Table 2.

The reference flow for this simulation is the pressure-driven MHD laminar flow in a rectangular duct with walls of finite conductivity [6]. However, the flow features deviate considerably from the reference.

Due to the complex topology of the magnetic field, the electric potential distribution in the fluid is no longer symmetric across the duct mid-plane. The induced currents modify their paths to be perpendicular to the magnetic field lines. The peak of the electric potential shifts toward the corners of the duct (see Fig. 4). Close to the opposite corners a weakening of the electric potential occurs and high velocity jets appear. The low conductivity ratio of the baffle enhances the jet nearby, whereas the opposite happens for the one close to the stiffener. In Fig. 5, the velocity contour is shown.

The fully developed state is maintained for most of the inlet duct with the currents confined to the flow cross-section. When the fluid approaches the bend, an axial potential difference appears driven by the velocity gradient between the fluid in the inlet duct and the bend. Axial currents are induced and the flow becomes 3D. In the outlet channel the intense magnetic field quickly restores the 2D flow.

For $M \gg 1$, inertial and viscous forces are confined to the boundary layers and the driving pressure gradient is balanced only by the Lorentz force. Thus, the streamlines of current density reported in Figure 5 are representative of pressure contours in the channel. For walls of uniform conductivity $M^{-1} \ll c \ll 1$, the pressure gradient can be expressed with the scaling law $dp/dz \propto \sigma_w u_0 B_0^2 \delta_w / L$ [2]. According to this relation and employing the computed results, the pressure drop in the channel for $M = 9800$ was estimated as $\Delta p \simeq 2055$ Pa.

5. Conclusions

A simplified analysis of the WCLL elementary cell was performed with the code ANSYS CFX for $M \leq 1000$. Relevant blanket features were modeled including skewed magnetic field and non uniform wall conductivity. Various interesting MHD phenomena were highlighted, among which an asymmetric potential distribution in the base duct and the formation of high velocity jets close to the baffle. The flow maintained the purely 2D state throughout the cell with axial currents and 3D flow confined to the bend. The channel pressure drop for the actual blanket magnetic

¹4 T(toroidal) and 1.175 T [?]]

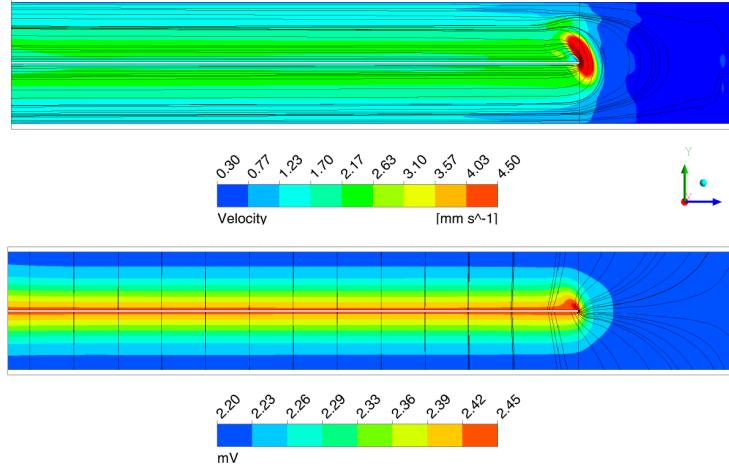


Fig. 5. Velocity (top) and electric potential contour with current streamlines (bottom) for the whole cell, radial-poloidal cross-section, at $M = 980$

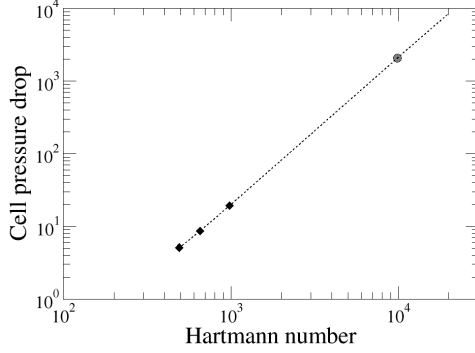


Fig. 6. Cell pressure drop plotted against M . Black diamonds mark the simulation results with the dashed line showing the correlation from [2]. Estimate at $M = 9800$ is indicated by the circle

field intensity ($M = 9800$) was estimated as $\Delta p \simeq 2055$ Pa. By comparison, the pressure drop computed for the hydraulic flow is $\Delta p = 0.05$ Pa.

The simulation results confirm that the expected pressure drop value in the elementary cell is not high enough to require insulating flow channel inserts (FCI) to decouple the fluid and the duct walls. However, a more detailed analysis is required to completely describe the cell MHD phenomena. Buoyancy forces due to the neutronic heating, the cooling pipes and the magnetic field gradient in the radial direction are expected to play an important role in the definition of the elementary cell MHD flow. Follow-up activities have been planned to integrate the result of this work, as well as the extension of the analysis to the manifold region.

Acknowledgements

This work has been carried out within the framework of the EUROfusion Consortium and has received funding

from the Euratom research and training programme 2014-2018 under grant agreement No 633053. The views and opinions expressed herein do not necessarily reflect those of the European Commission.

References

References

- [1] A. Del Nevo, E. Martelli, P. Agostini, P. Arena, G. Bongiovì, G. Caruso, G. Di Gironimo, P. Di Maio, M. Eboli, R. Giammusso, et al., WCLL breeding blanket design and integration for 2015: status and perspectives, *Fusion Engineering and Design* doi: 10.1016/j.fusengdes.2017.03.020.
- [2] S. Smolentsev, et al., MHD thermofluid issues of liquid-metal blankets: phenomena and advances, *Fusion Engineering and Design* 85 (7) (2010) 1196–1205.
- [3] S. Smolentsev, et al., An approach to verification and validation of MHD codes for fusion applications, *Fusion Engineering and Design* 100 (2015) 65–72.
- [4] P. A. Davidson, *An introduction to magnetohydrodynamics*, vol. 25, Cambridge university press, 2001.
- [5] L. Bühler, Laminar buoyant magnetohydrodynamic flow in vertical rectangular ducts, *Physics of Fluids (1994-present)* 10 (1) (1998) 223–236.
- [6] J. Hunt, Magnetohydrodynamic flow in rectangular ducts, *Journal of Fluid Mechanics* 21 (04) (1965) 577–590.
- [7] J. Shercliff, Steady motion of conducting fluids in pipes under transverse magnetic fields, in: *Mathematical Proceedings of the Cambridge Philosophical Society*, vol. 49, Cambridge University Press, 136–144, 1953.
- [8] I. Di Piazza, L. Bühler, A general computational approach for magnetohydrodynamic flows using the CFX code: buoyant flow through a vertical square channel, *Fusion Science and Technology* 38 (2) (2000) 180–189.
- [9] C. Mistrangelo, L. Bühler, Numerical Study of Fundamental Magnetoconvection Phenomena in Electrically Conducting Ducts, *IEEE Transactions on Plasma Science* 40 (3) (2012) 584–589.
- [10] A. Tassone, F. Giannetti, G. Caruso, Numerical study of laminar magneto-convection in a differentially heated square duct, *Journal of Physics: Conference Series* 796 (1) (2017) 012004, doi: 10.1088/1742-6596/796/1/012004.
- [11] U. Jauch, V. Karcher, B. Schulz, G. Haase, *Thermophysical properties in the system Li-Pb*, 1986.

- [12] K. Mergia, N. Boukos, Structural, thermal, electrical and magnetic properties of Eurofer 97 steel, *Journal of Nuclear Materials* 373 (1) (2008) 1–8.